

Adaptive Neural Layer for Globally Filtered Segmentation

Viktor Shipitsin*, Iaroslav Beshpalov*, Dmitry V. Dylov†

Skolkovo Institute of Science and Technology

Bolshoy blvd., 30/1, Moscow, Russia 121205

{Viktor.Shipitsin, Iaroslav.Beshpalov, d.dylov}@skoltech.ru

Abstract

This study is motivated by typical images taken during ultrasonic examinations in the clinic. Their grainy appearance, low resolution, and poor contrast demand an eye of a very qualified expert to discern targets and to spot pathologies. Training a segmentation model on such data is frequently accompanied by excessive pre-processing and image adjustments, with an accumulation of the localization error emerging due to the digital post-filtering artifacts and due to the annotation uncertainty. Each patient case generally requires an individually tuned frequency filter to obtain optimal image contrast and to optimize the segmentation quality. Thus, we aspired to invent an adaptive global frequency-filtering neural layer to “learn” optimal frequency filter for each image together with the weights of the segmentation network itself. Specifically, our model receives the source image in the spatial domain, automatically selects the necessary frequencies from the frequency domain, and transmits the inverse-transform image to the convolutional neural network for concurrent segmentation. In our experiments, such “learnable” filters boosted typical U-Net segmentation performance by 10% and made the training of other popular models (DenseNet and ResNet) almost twice faster. In our experiments, this trait holds both for two public datasets with ultrasonic images (breast and nerves), and for natural images (Caltech birds).

1. Introduction

Ultrasound is one of the most popular imaging modalities in the medical field due to the fact that it is inexpensive, non-invasive, safe, accessible, and entails no ionizing radiation [1]. Today, the analysis of various formations in the images is carried out by each doctor individually and the in-

terpretation of the information content in the images is extremely operator-dependent. With the development of computer vision technologies, implementation of the algorithms to assist doctors in analyzing the ultrasound images is a noticeable trend in the biomedicine [2, 3]. On the other hand, computer scientists eagerly accepted interesting challenges posed by the nature of the ultrasonic data, with one such challenge being the automatic image segmentation problem.

When medical image segmentation is concerned, one naturally starts with the U-Net encoder-decoder like models [4]. At the moment, there are various modifications that prove efficient in various scenarios: Attention U-Net [5], U-Net++ [6, 7], U-Net 3+ [8]. In addition to U-Net family of architectures, ResNet and DenseNet models are also frequently employed for the purpose of segmentation [9, 10].

However, none of the above approaches uses the fact that ultrasound has a wave nature. Internal organs and tissues of a human are able to reflect an echo, for example, to return a signal during ultrasound examination, that is, they have echogenicity. Depending on the high or low echogenicity in the ultrasound image, we will see lighter or darker colors, respectively [11]. The frequency domain of such a study carries a lot of information that we want to use for segmentation of ultrasound images. Thus, by changing the frequencies in the Fourier spectrum of the image, we can distinguish abnormal formations among other natural ones in the area under study.

Using the direct and inverse Fourier transform, we can go from the spatial domain of the image description to the frequency domain and vice versa. In the frequency spectrum, specific frequencies are responsible for different properties of the image, which can be extracted with filtering. For example the high-pass filter is used for edge detection, visualizing details, the low-pass filter for reduction of outliers and of contrast, i.e. a smoothing effect. In this article, we provide an algorithm that improves the quality and efficiency of existing popular segmentation algorithms by automatically finding a global filter, which will leave only those fre-

*Contributed equally.

†Corresponding author.

quencies that improve segmentation as a whole. We demonstrate our experiments on two different ultrasound datasets: the Breast Ultrasound Images Dataset (Dataset BUSI) [12], where the ultrasound scans of breast cancer, which are categorized into three classes: normal, benign, and malignant and the BPUI dataset [13], where there are challenged to build a model that can identify nerve structures called the Brachial Plexus (BP) in ultrasound images of the neck. At the end of our research with medical images, it was decided to check how the proposed approach would affect the classic dataset. An open Caltech dataset of birds [14] was used. As it turned out, filtering the frequency spectrum speeds up convergence on non-medical data. This may be due to the fact that light is by nature also a wave, and the presentation of frequency information in an explicit form allows the network to navigate more quickly and find key patterns and matches in the data.

Related Work. At present, the idea of additional use of other spaces to improve the quality of neural networks has been rapidly developing. Fourier analysis has been successfully used for dynamic structure segmentation problems, where dynamic structures were distinguished using only the phase spectrum [15].

Semantic segmentation using domain adaptation, where the frequency amplitudes of the source and target images are combined [16], and various high-frequency low-dimensional regression problems, where Fourier features improved the results of coordinate-based multilayer perceptrons for image regression, 3D shape regression, MRI reconstruction, inverse rendering tasks [17]. The above works have shown their effectiveness, that really some information can be lost when using only the spatial domain. However, existing algorithms do not consider the selection of the required spectrum as data preprocessing. The difficulty is that manually selecting the correct frequency filter is not a simple task. Therefore, our solution is for the segmentation model to automatically select the weights for transforming the frequency spectrum for each specific task. As a result, proposed approach performs the denoising process automatically, since it results in the removal of "unnecessary" noise frequencies depending on the provided data set and improve quality of the different models in segmentation tasks.

2. Datasets

To test suggested method, the three different datasets, two of which have the nature of ultrasound (US), were used (Fig. 1).

US data is collected on the basis of the reception of the echo signal reflected from the surfaces of tissues of different density, in proportion to the difference in resistance. depending on echogenicity (ability to reflect or transmit US

waves), different types of structures are distinguished in the scans:

- Hyperechoic (white regions on the scan)
- Hypoechoic (gray regions on the scan)
- Anechoic (black regions on the scan)

For example, muscles are hypoechoic with striate structure, and the nerves are hyperechoic with stippled structure.

Unfortunately, when segmentation of such data by a person, a misinterpretation takes place due to the following features and artifacts:

- high or midrange (5-15 MHz) and low (2-5 MHz) frequency probes provide better resolution or penetration, but not both at once;
- reverberation, that occurs when an ultrasound beam encounters two strong parallel reflectors;
- acoustic shadowing resulting from structures that strongly absorb or reflect ultrasonic waves;
- increased echoes deep to structures that transmit sound exceptionally well.

Therefore, correct data processing should lead to better quality of data analysis (segmentation) using computer vision models.

Dataset BUSI [12]. This dataset contains medical ultrasound images of breast cancer for different female patients, along with ground truth masks. Data collected to address the problem of classification, detection, and segmentation of breast cancer, one of the most common causes of death in women worldwide. Therefore, all images are divided into three classes: normal, with benign or malignant tumor.

Brachial Plexus Ultrasound Images [13]. This set is intended for the task of segmentation of a nerves network, formed by the anterior branches of the four lower cervical nerves and the first thoracic nerve, called the brachial plexus (BP). Recognition of nerve structures on ultrasound scans is an important step when inserting a patient's pain management catheter. The dataset contains both images with plexuses and without, as well as a ground truth masks.

In the third dataset, a set is formed according to a general principle for solving various computer vision problems for images of a certain category.

Caltech Birds (2011) Dataset [14]. This dataset provides photographs of 200 different, mainly North American, bird species, organized by scientific classification. Annotations, which were obtained as the median over locations for 5 different users per image, include bounding boxes, segmentation labels. Therefore, for the current work, only the core (main) contours of the segmentation labels are remained in ground truth masks.

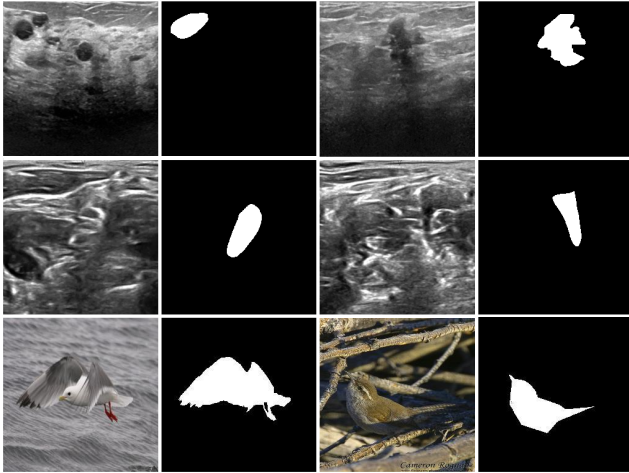


Figure 1. Datasets with poorly discernible objects considered in our work. First two rows: Ultrasound imaging data [BUSI (breast [12]) and BPUI (nerves [13])], third row: natural images (Caltech birds [14]).

3. Method

Data preprocessing is an essential part of any computer vision algorithms. The most common methods are based on the representation of an image in a computer. However, we pay attention to the method of obtaining data, that is, the physical essence. Considering the image in frequency space, we try to account for the physics of ultrasound examination. Further, the frequency analysis is carried out in an automatic mode, taking into account the entire model, which allows the algorithm to take into account the specifics of the problem presented in the training data set.

The method proposed herein is based on deep learning approach. We provide the concept of a trainable layer, which will be trained together with the selected model to solve the problem of segmentation of ultrasound images. By placing this layer in front of the baseline of the model, the algorithm will automatically select weights for frequency filtering of images at the input to the model.

Fourier analysis has been successfully used for different dynamic structure. With the Fourier transform, it is possible to move from the frequency domain to the spatial and vice

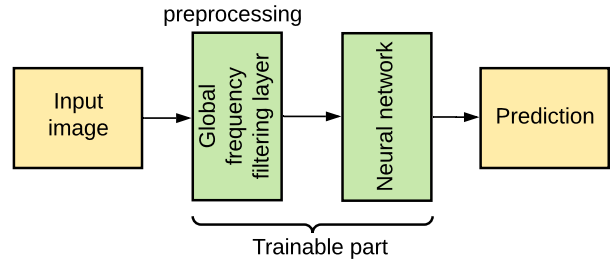


Figure 2. Block diagram of the proposed method. Adaptive Neural Layer allows for global filtering to be trained along with the weights of the main model.

versa without lost of information. The Fourier transform appears when considering the Fourier series of a function with an unbounded domain. The Fourier transform has the properties of linearity, preserving the accuracy of signal approximation (Parseval's theorem), which are preserved when the signal is represented using discrete vectors. If we represent the image as a two-dimensional signal, then making an alternating one-dimensional Fourier transform, first by rows, then by columns (or vice versa), we obtain a description of the image in the frequency domain [18]. Denoting $W_n = e^{i\frac{2\pi}{n}}$, we can write the expression as follows:

$$\hat{\mathbf{I}}(u, v) = \frac{1}{N_{\text{cols}}N_{\text{rows}}} \sum_{x=0}^{N_{\text{cols}}-1} \sum_{y=0}^{N_{\text{rows}}-1} \mathbf{I}(x, y)W_{N_{\text{cols}}}^{-xu}W_{N_{\text{rows}}}^{-yv}$$

where $\mathbf{I}(x, y)$ - original image (spatial description), $\hat{\mathbf{I}}(u, v)$ - frequency domain image.

The main method of visual analysis of Fourier transformation is to calculate its spectrum, i.e. coordinate-wise absolute value $\|\hat{\mathbf{I}}(u, v)\|_2$, or energy spectrum $\|\hat{\mathbf{I}}(u, v)\|_2^2$. To filter image in the frequency domain we need to take a function that modifies spectrum in a specific way. Another important property of the Fourier transform is described by the convolution theorem [19]: we can select both the kernel filter in the spatial domain and the global (kernel with the same dimensions as the image) filter in the frequency domain, which will do the same transformations, however, in the first case we deprive ourselves of the possibility of applying direct frequency-dependent filtering functions as in the second case [20].

In the frequency domain, there is flexibility in designing filtering functions. We can independently indicate which of the selected frequencies to suppress or enhance. However, due to the wide variety of options and the specificity of each task, it is very difficult to select the appropriate filter manually. The proposed algorithm of the trained filtering layer is capable of forming a more complex and task-specific filter,

than presented in the Figure 3. Another argument in favor of using such filtering is the availability of efficient algorithms for fast Fourier transform (FFT) and element-wise multiplication.

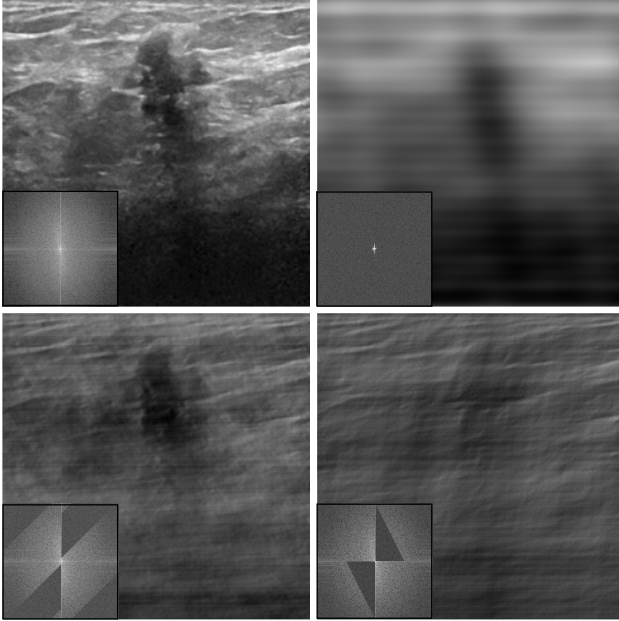


Figure 3. The result of applying different frequency filters to the original ultrasound image (top left). Insets in the corner show corresponding Fourier spectra. Notice emergence of different scales and textures after the filtering, which had motivated us to include the search of the best filtering into the optimization problem.

We are trying to find a global filter, which will leave only those frequencies that improve segmentation as a whole. We may decide on a high-pass filter, in which high frequencies are passed and low frequencies are significantly reduced, for example for edge detection, visualizing details or a low-pass filter for reduction of outliers and of contrast, i.e. a smoothing effect. For each task, you need your own filter, which will not be easy to select manually. Therefore, we can give the task of filter selection to the computer by integrating the appropriate adaptive neural layer for global frequency filtering, which will be trained along with the entire model. It's obvious that such a global filter is a non-linear function from the frequency domain. So we need to approximate this non-linear function. Below we will describe algorithm for constructing a training layer, based on the above provisions.

To approximate an arbitrary nonlinear function, a neural network with just one hidden layer is enough. Therefore, we can achieve a general form of the transform function, which is adaptive to each frequency, with following expression:

$$\|\hat{\mathbf{I}}(u, v)\|_2 \leftarrow W_2 * \sigma\left(W_1 * \|\hat{\mathbf{I}}(u, v)\|_2 + B_1\right) + B_2,$$

where $\hat{\mathbf{I}}(u, v)$ - frequency domain image, W_1, W_2 - trained weight matrices (non-negative), B_1, B_2 - trained bias matrices (non-negative), $\sigma(\cdot)$ - some nonlinear activation function and $*$ - element-wise multiplication (Algorithm 1).

Algorithm 1: Global Frequency Filtering Layer

$W_1, W_2, B_1, B_2 \leftarrow ReLU(W_1), ReLU(W_2),$
 $ReLU(B_1), ReLU(B_2), rfft$ - Fast Fourier Transform
for real input

input: x - initial ultrasound image

1: $rft_x \leftarrow rfft(x)$

2: $spectrum \leftarrow W_2 * \sigma\left(W_1 * \|rft_x\|_2 + B_1\right) + B_2$

3: $rft_x \leftarrow spectrum * \left(rft_x / \|rft_x\|_2\right)$

4: $x \leftarrow inverse_rfft(x)$

output: x - ultrasound image after applying a layer of global frequency filtering

4. Experiments

Learning process. In this research work, the *Combined Loss* function of *Dice Loss* and *Cross Entropy Loss* with approximately equal weights (0.6 and 0.4 respectively), which were optimized with *Adam* optimizer with *learning rate* = 0.001, is used. To evaluate the quality of segmentation, the *Dice coefficient* [21], which, in essence, measures the proportion of the intersection area of the predicted and trustworthy pixels in relation to the total area is applied.

Activation Functions. The activation function used in the global filtering layer is a hyperparameter that needs to be selected depending on the problem being solved and the dataset. In the provided algorithm, the function receives a non-negative matrix as input, it's due to the fact that the frequency with negative weight has no physical interpretation. Therefore, several popular activation functions have been selected and investigated. The results of the study are presented in the Table 1. As can be seen from the results, the activation function plays an important role. The difference between the best and worst activation function in some cases is about 10% by metric. It should be noted that the activation functions *Mish* and *ReLU* have shown themselves well on all datasets. So *Mish* and *ReLU* are good for using the algorithm out of the box. Further experiments were carried out using *ReLU* activation function.

Different Models Comparison. To test the proposed method, three different models were taken as a basis:

Table 1. Validation Dice score for different activation functions on the BUSI and BPUI datasets in the general layer. Red color font corresponds to the worst score, and black bold font corresponds to the best score.

ACTIVATION FUNCTION	BUSI			BPUI		
	U-NET	DENSENET	RESNET	U-NET	DENSENET	RESNET
SIGMOID	0.70	0.82	0.83	0.68	0.75	0.72
RELU	0.77	0.84	0.83	0.75	0.77	0.75
RELU6	0.76	0.83	0.81	0.73	0.76	0.74
SOFTPLUS	0.74	0.83	0.82	0.70	0.75	0.74
TANH	0.75	0.83	0.83	0.73	0.76	0.74
SWISH ($\beta = 1.0$)	0.78	0.81	0.80	0.74	0.76	0.75
MISH	0.78	0.83	0.82	0.75	0.77	0.75

- U-Net - the first successful architecture in biomedical image segmentation. The core idea behind U-Net is to use advantage of rich feature representation from convolutional networks and combine it with lower level image representation (that is solved by using skip connections).
- model with densenet encoder, which contains shorter connections between layers close to the input and those close to the output for more accurate and efficient teaching.
- model with resnet encoder, where the layers are reformulated as learning residual functions with reference to the layer inputs, instead of learning unreferenced functions.

Further, these models were considered with the addition of various configurations of the denoising layer.

For the *Linear* configuration a simple single layer neural network was used. For the *Linear log* and *Genral log* configurations log-transformed spectrum was used, and in the linear case, the exponential transformation was additionally applied:

$$\|\hat{\mathbf{I}}(u, v)\|_2 \leftarrow \exp \left[W * \log (1 + \|\hat{\mathbf{I}}(u, v)\|_2) \right] - 1,$$

where W - trained weight matrix (non-negative) and $*$ - element-wise multiplication. Thus, we compare the segmentation results of the base model and the model with the addition of one of the types of proposed trainable denoising layer. Thus, when adding the proposed trainable preprocessing layer, filtered data is fed to the input of each base model (Fig. 4).

Models are trained using the following hyperparameters: *image size* = (256, 256) - model image input size (height, width) and *batch size* = 4; for U-Net: *init_features* = 32 - number of channels (features) in initial convolution, *depth*

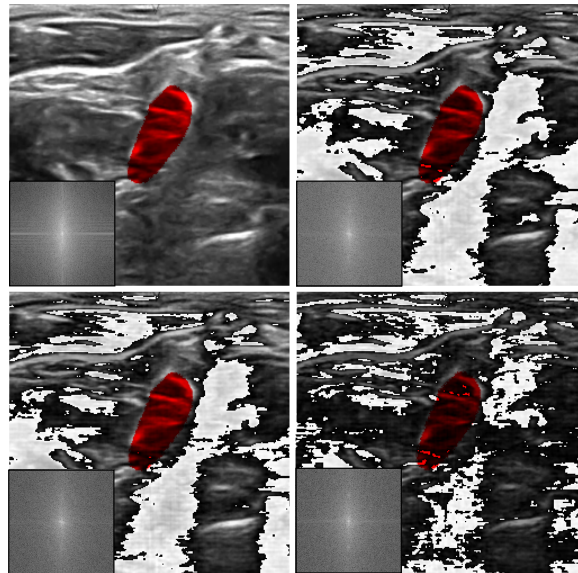


Figure 4. Examples of trained filters and their effect on the segmentation. Top left: original image and ground truth mask; top right: linear filter; bottom left: general filter; bottom right: general log filter. Insets in the corner show corresponding spectra.

= 3 - number of downsteps; for DenseNet (as for densenet-121): *num_init_features* = 32 - number of channels (features) in initial convolution, *growth_rate* = 32 - how many filters to add each layer, *block_config* = 6, 12, 24, 16 - how many layers in each pooling block; for ResNet (as for resnet-18): *blocks*: 2, 2, 2, 2 - how many layers in each pooling block. The numerical results of validation metrics for all experiments are collected in the Table 2.

Specifics of Ultrasound Datasets. In datasets collected using ultrasound imaging, there are a lot of negative examples (with a zero or an empty mask). Unlike the Caltech Birds dataset, such data require more focus, dedication,

Table 2. Validation Dice score compared for different models on the BUSI, BPUI and Caltech Birds datasets. The worst model is shown in red font, the best model is shown in black bold font.

MODEL	BUSI	BPUI	CALTECH BIRDS
U-NET	0.70±0.01	0.58±0.01	0.82±0.01
* FOURIER LINEAR	0.71±0.01	0.62±0.01	0.86±0.01
* FOURIER LINEAR LOG	0.71±0.01	0.62±0.01	0.86±0.01
* FOURIER GENERAL	0.75±0.01	0.75±0.02	0.86±0.01
* FOURIER GENERAL LOG	0.75±0.01	0.75±0.02	0.86±0.01
DENSENET	0.76±0.01	0.72±0.01	0.94±0.01
* FOURIER LINEAR	0.78±0.01	0.75±0.01	0.94±0.01
* FOURIER LINEAR LOG	0.78±0.01	0.77±0.01	0.94±0.01
* FOURIER GENERAL	0.81±0.01	0.76±0.02	0.94±0.01
* FOURIER GENERAL LOG	0.77±0.01	0.73±0.02	0.94±0.01
RESNET	0.78±0.01	0.70±0.01	0.93±0.01
* FOURIER LINEAR	0.80±0.01	0.72±0.01	0.94±0.01
* FOURIER LINEAR LOG	0.80±0.01	0.72±0.02	0.94±0.01
* FOURIER GENERAL	0.81±0.01	0.74±0.02	0.94±0.01
* FOURIER GENERAL LOG	0.81±0.01	0.74±0.02	0.94±0.01

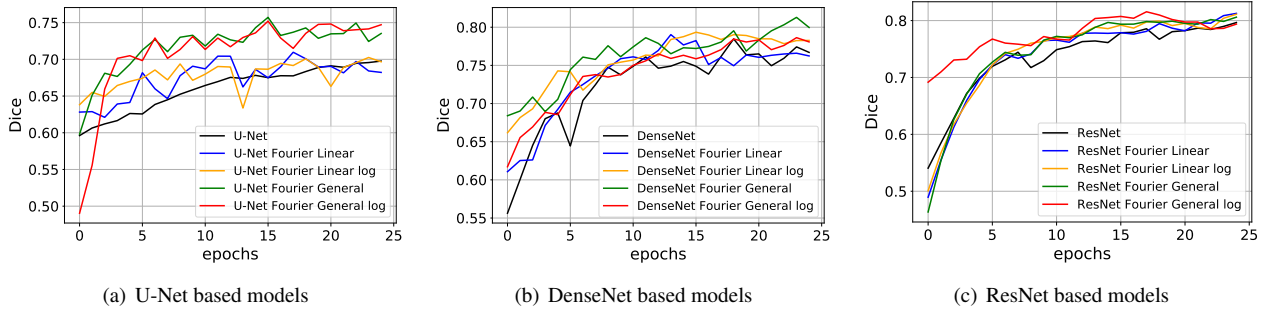


Figure 5. Dice score on the validation set during training on the BUSI dataset.

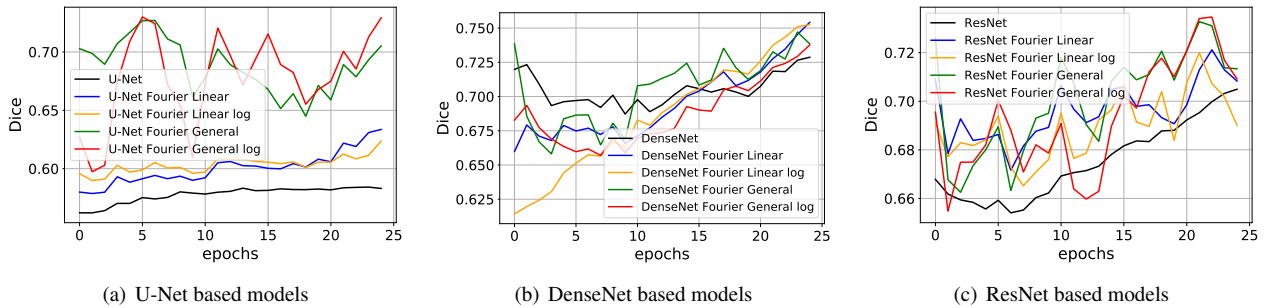


Figure 6. Dice score on the validation set during training on the BPUI dataset.

and expertise to annotate them with labels. But, as with all human-tagged data, one should expect artifacts and potential errors in the markings: for example, the BP data has been annotated by pseudo-experts (people who have been

trained and instructed by experts).

Figures 5, 6, 7 portray different behavior of the Dice score metrics during training on the three datasets described above, and the corresponding loss functions are shown in

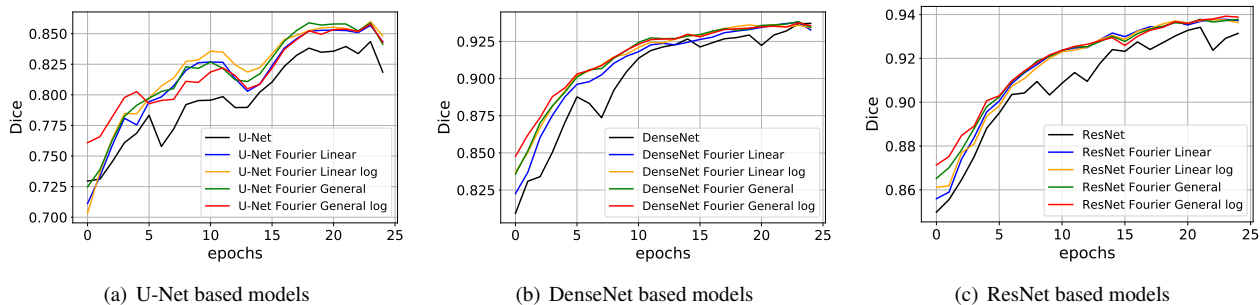


Figure 7. Dice score on the validation set during training on the Caltech Birds dataset.

the Supplementary material.

Several important observations can be made:

- the observed improvement of Dice score on the ultrasound datasets depends on the number of parameters of the base model: the larger the architecture size, the less noticeable the increase in the metric when using the adaptive layer;
- on the natural images dataset, there is a faster convergence of all models when the proposed filtering layer is added, than in any of the base models.
- The proposed log operation applied to the spectra allows for the small pixel values and eliminates fluctuation artifacts otherwise appearing from the truncation.
- Addition of the adaptive filter to the natural images provides “smoother” convergence of the training curves. We believe this trait could be instrumental for accelerating many state-of-the-art models where predicting the behaviour of the model is important (e.g., reinforcement and/or active learning).

5. Conclusions

The method proposed in our work proved to be efficient on all datasets and all classical model architectures that we have considered. In all cases, the use of simple adaptive frequency filtering layer has led to faster convergence of the training process than in the case of the stand-alone model, having shown higher segmentation quality both on train and on test samples. A rather important finding is the increase of Dice score for the case of simple U-Net by more than 10% when the adaptive global filter is added. This promises an opportunity for the areas, such as medicine, where getting marked data is an acknowledged challenge, causing one to attempt learning on small datasets. In these cases, the use of heavy models with a large number of parameters is one possible solution which frequently leads to a fast overfit; whereas, addition of simple adaptive filtering layers “trims” unnecessary frequencies in the Fourier domain and makes

the model learn only the vital frequencies along with the weights of the main neural network. All of this is accomplished while optimizing the targeted advantage function of interest to a particular application (e.g., Dice score in our case).

The convergence speed of models plays an important role too. Areas, such as ultrasound imaging, entail big amounts of data, the labelling of which takes a lot of time and requires the involvement of highly qualified experts. Due to this, in computer vision is relevant task of active learning [22], which implies the further retraining of models. Same applies to tasks which entail unsupervised segmentation [23]. Our adaptive global filtering layer can significantly reduce the number of necessary epochs for training convergence without losing (or sometimes even with boosting) the quality of the model in such modern research areas as active learning, where the models are re-trained iteratively and ultimately allow for the time gain. Initially, we anticipated that our adaptive layer would improve convergence and quality primarily in the ultrasound data (the echogenic nature of which is known to be prone to high sensitivity to the frequency knobs). But we were surprised to find out the improvement in the natural images as well. This expands the possible areas of application of the proposed approach and opens up a new direction of research of adaptive layers (e.g., in more complex multi-layer architectures [24], in generative and image translation models [25], in learnable frequency kernels [26], in iterative anomaly detection models [27], etc. Lightening of these models via a simple adaptive filtering layer holds potential for a seamless integration in various computer vision applications.).

References

- [1] Vikas Chaudhary and Shahina Bano. Thyroid ultrasound. *Indian journal of endocrinology and metabolism*, 17:219–27, 03 2013. 1
- [2] Junho Song, Young Jun Chai, Hiroo Masuoka, Sun-Won Park, Su-jin Kim, June Choi, Hyoun-Joong Kong, Kyu Eun Lee, Joongseek Lee, Nojun Kwak, Ka Yi, and Akira Miyachi. Ultrasound image analysis using deep learning

- algorithm for the diagnosis of thyroid nodules. *Medicine*, 98:e15133, 04 2019. 1
- [3] Lei Wang, Shujian Yang, Shan Yang, Cheng Zhao, Guangye Tian, Yuxiu Gao, Yongjian Chen, and Yun Lu. Automatic thyroid nodule recognition and diagnosis in ultrasound imaging with the yolov2 neural network. *World Journal of Surgical Oncology*, 17, 12 2019. 1
- [4] Olaf Ronneberger, Philipp Fischer, and Thomas Brox. U-net: Convolutional networks for biomedical image segmentation. *CoRR*, abs/1505.04597, 2015. 1
- [5] Ozan Oktay, Jo Schlemper, Loïc Le Folgoc, Matthew C. H. Lee, Mattias P. Heinrich, Kazunari Misawa, Kensaku Mori, Steven G. McDonagh, Nils Y. Hammerla, Bernhard Kainz, Ben Glocker, and Daniel Rueckert. Attention u-net: Learning where to look for the pancreas. *CoRR*, abs/1804.03999, 2018. 1
- [6] Zongwei Zhou, Md Mahfuzur Rahman Siddiquee, Nima Tajbakhsh, and Jianming Liang. Unet++: A nested u-net architecture for medical image segmentation. *CoRR*, abs/1807.10165, 2018. 1
- [7] Z. Zhou, M. M. R. Siddiquee, N. Tajbakhsh, and J. Liang. Unet++: Redesigning skip connections to exploit multiscale features in image segmentation. *IEEE Transactions on Medical Imaging*, 39(6):1856–1867, 2020. 1
- [8] Huimin Huang, Lanfen Lin, Ruofeng Tong, Hongjie Hu, Zhang Qiaowei, Yutaro Iwamoto, Xian-Hua Han, Yen-Wei Chen, and Jian Wu. Unet 3+: A full-scale connected unet for medical image segmentation. 04 2020. 1
- [9] Gao Huang, Zhuang Liu, and Kilian Q. Weinberger. Densely connected convolutional networks. *CoRR*, abs/1608.06993, 2016. 1
- [10] Kaiming He, Xiangyu Zhang, Shaoqing Ren, and Jian Sun. Deep residual learning for image recognition. *CoRR*, abs/1512.03385, 2015. 1
- [11] Barys Ihnatsenka and Andre Boezaart. Ultrasound: Basic understanding and learning the language. *International journal of shoulder surgery*, 4:55–62, 07 2010. 1
- [12] Walid Al-Dhabyani, Mohammed Gomaa, Hussien Khaled, and Aly Fahmy. Dataset of breast ultrasound images. *Data in Brief*, 28:104863, 11 2019. 2, 3
- [13] <https://www.kaggle.com/c/ultrasound-nerve-segmentation/data>. 2, 3
- [14] C. Wah, S. Branson, P. Welinder, P. Perona, and S. Belongie. The Caltech-UCSD Birds-200-2011 Dataset. Technical Report CNS-TR-2011-001, California Institute of Technology, 2011. 2, 3
- [15] Jianghong Li, Liang Chen, and Yuanhu Cai. Dynamic texture segmentation using fourier transform. *Modern Applied Science*, 3, 08 2009. 2
- [16] Yanchao Yang and Stefano Soatto. Fda: Fourier domain adaptation for semantic segmentation. 04 2020. 2
- [17] Matthew Tancik, Pratul Srinivasan, Ben Mildenhall, Sara Fridovich-Keil, Nithin Raghavan, Utkarsh Singhal, Ravi Ramamoorthi, Jonathan Barron, and Ren Ng. Fourier features let networks learn high frequency functions in low dimensional domains. 06 2020. 2
- [18] Steven Brunton and J. Kutz. *Data-Driven Science and Engineering: Machine Learning, Dynamical Systems, and Control*. 01 2019. 3
- [19] J.M. Blackledge. *Digital Image Processing: Mathematical and Computational Methods*. 11 2005. 3
- [20] Reinhard Klette. *Concise Computer Vision: An Introduction into Theory and Algorithms*. Springer Publishing Company, Incorporated, 2014. 3
- [21] Fausto Milletari, Nassir Navab, and Seyed-Ahmad Ahmadi. V-net: Fully convolutional neural networks for volumetric medical image segmentation. 06 2016. 4
- [22] Artem Shelmanov, Vadim Liventsev, Danil Kireev, Nikita Khromov, Alexander Panchenko, Irina Fedulova, and Dmitry V Dylov. Active learning with deep pre-trained models for sequence tagging of clinical and biomedical texts. In *2019 IEEE International Conference on Bioinformatics and Biomedicine (BIBM)*, pages 482–489. IEEE, 2019. 7
- [23] Iaroslav Bespalov, Nazar Buzun, and Dmitry V Dylov. Brulé: Barycenter-regularized unsupervised landmark extraction. *arXiv preprint arXiv:2006.11643*, 2020. 7
- [24] Aritra Chowdhury, Dmitry V Dylov, Qing Li, Michael MacDonald, Dan E Meyer, Michael Marino, and Alberto Santamaria-Pang. Blood vessel characterization using virtual 3d models and convolutional neural networks in fluorescence microscopy. In *2017 IEEE 14th International Symposium on Biomedical Imaging (ISBI 2017)*, pages 629–632. IEEE, 2017. 7
- [25] Denis Prokopenko, Joël Valentin Stadelmann, Heinrich Schulz, Steffen Renisch, and Dmitry V Dylov. Unpaired synthetic image generation in radiology using gans. In *Workshop on Artificial Intelligence in Radiation Therapy*, pages 94–101. Springer, Cham, 2019. 7
- [26] Elizaveta Lazareva, Oleg Rogov, Olga Shegai, Denis Larionov, and Dmitry V Dylov. Learnable hollow kernels for anatomical segmentation. *arXiv preprint arXiv:2007.05103*, 2020. 7
- [27] Nina Tuluptceva, Bart Bakker, Irina Fedulova, Heinrich Schulz, and Dmitry V Dylov. Anomaly detection with deep perceptual autoencoders. *arXiv preprint arXiv:2006.13265*, 2020. 7

Supplementary material

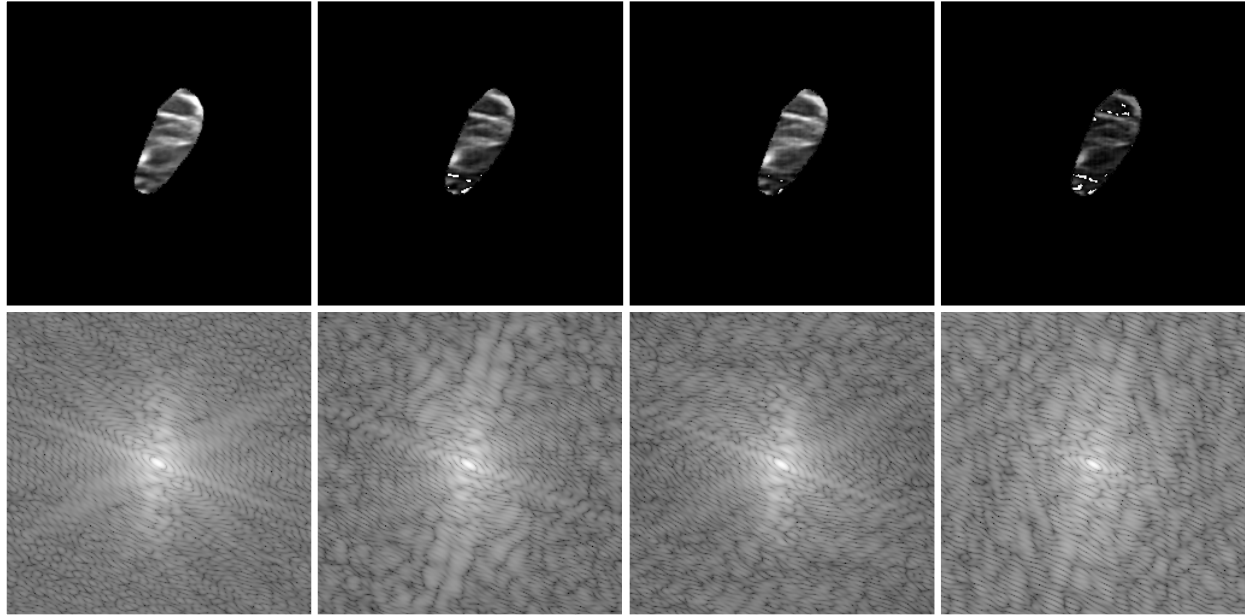


Figure 8. Example of trainable filter application to mask area. initial image, linear filter, general filter, general log filter.

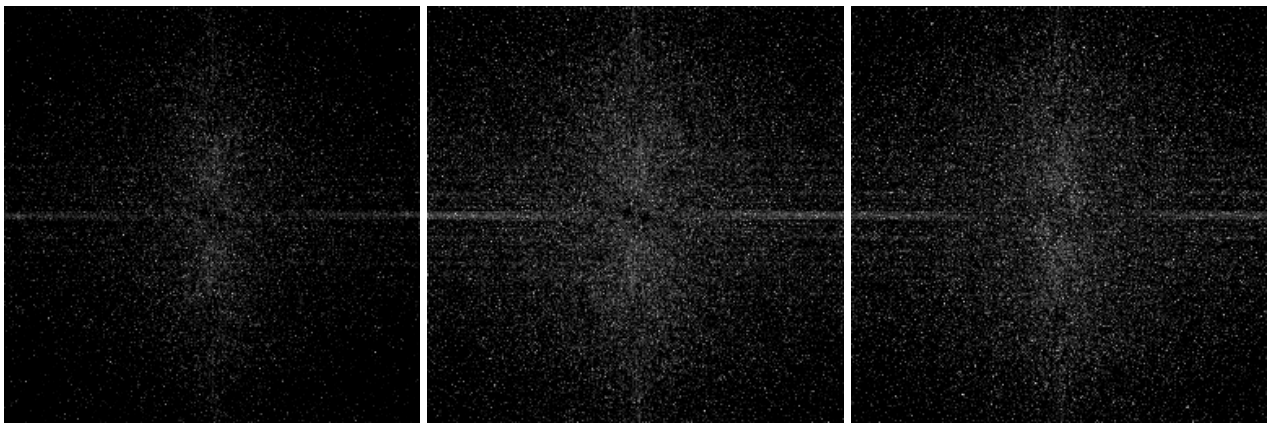
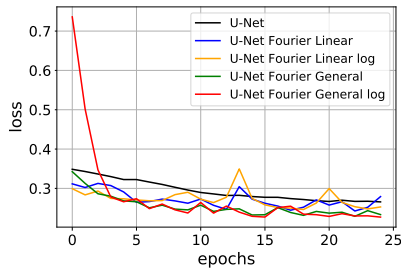
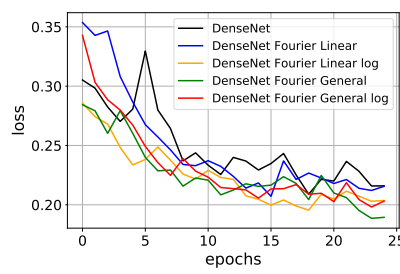


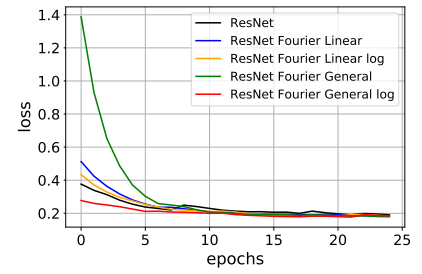
Figure 9. Frequency difference between linear filter, general filter, general log filter and initial spectrum.



(a) U-Net based models

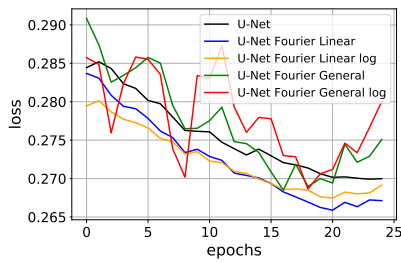


(b) DenseNet based models

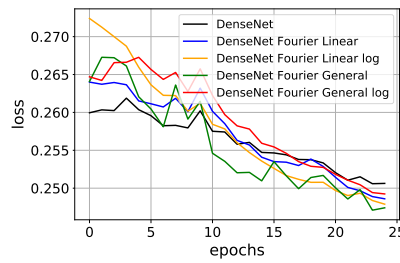


(c) ResNet based models

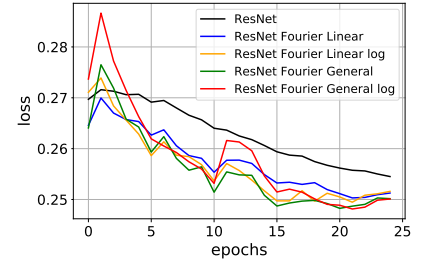
Figure 10. Loss function on validation set during train process on the BUSI dataset.



(a) U-Net based models

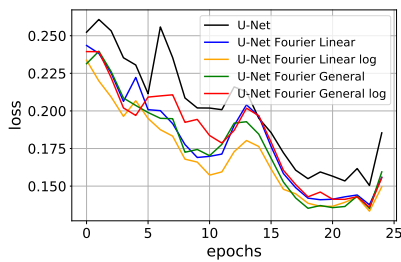


(b) DenseNet based models

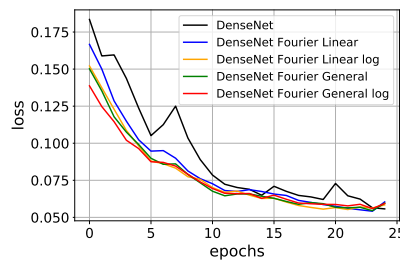


(c) ResNet based models

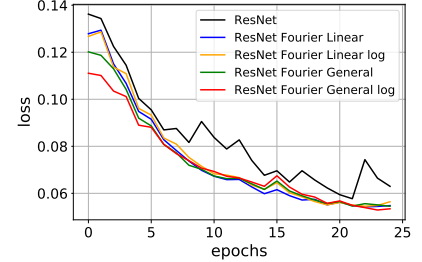
Figure 11. Loss function on validation set during train process on the BPUI dataset.



(a) U-Net based models



(b) DenseNet based models



(c) ResNet based models

Figure 12. Loss function and metrics on validation set during train process on the Caltech Birds dataset.